# High-field ESR spectroscopy of the spin dynamics in La1-xSrxMnO3 (x <~ 0.175)

**D. Ivannikov, Markus Biberacher, Hans-Albrecht Krug von Nidda, Andrei Pimenov, Alois Loidl, A. A. Mukhin, A. M. Balbashov**

**Angaben zur Veröffentlichung / Publication details:**

Ivannikov, D., Markus Biberacher, Hans-Albrecht Krug von Nidda, Andrei Pimenov, Alois Loidl, A. A. Mukhin, and A. M. Balbashov. 2002. "High-field ESR spectroscopy of the spin dynamics in La1-xSrxMnO3 (x <~ 0.175)." *Physical Review B* 65 (21): 214422. https://doi.org/10.1103/PhysRevB.65.214422.



# High-field ESR spectroscopy of the spin dynamics in $La_{1-x}Sr_xMnO_3$ ($x \leqslant 0.175$)

D. Ivannikov, M. Biberacher, H.-A. Krug von Nidda, A. Pimenov,* and A. Loidl
*Experimentalphysik V, Elektronische Korrelationen und Magnetismus, Institut für Physik, Universität Augsburg, 86135 Augsburg, Germany*

A. A. Mukhin
*General Physics Institute of the Russian Academy of Sciences, 119991 Moscow, Russia*

A. M. Balbashov
*Moscow Power Engineering Institute, 105835 Moscow, Russia*

(Received 1 February 2002; published 4 June 2002)

High-field electron-spin-resonance (ESR) experiments have been carried out in single crystals of $La_{1-x}Sr_xMnO_3$ in the concentration range $0 \leqslant x \leqslant 0.175$. Different quasioptical arrangements have been utilized for frequencies $40 \leqslant \nu \leqslant 700$ GHz and for magnetic fields $B \leqslant 12$ T. A splitting of the antiferromagnetic resonance (AFMR) mode is observed in the magnetic field for the parent compound $LaMnO_3$, in agreement with the antiferromagnetic structure of this material. Abrupt changes in the AFMR frequencies have been observed around $x \simeq 0.025$, and were attributed to a transition between a pure antiferromagnetic and a canted state. For increasing Sr doping the observed AFMR modes are split even in a zero field, which can be naturally explained using a concept of a canted magnetic structure for $x < 0.1$. In $La_{0.825}Sr_{0.175}MnO_3$ the ESR spectra are consistent with the ferromagnetic and metallic state. The lines of ferromagnetic resonance and ferromagnetic antiresonance can be clearly observed. For intermediate concentrations $0.1 \leqslant x \leqslant 0.15$ complicated ESR spectra were observed, which can be well explained by a single ferromagnetic resonance mode and taking electrodynamic effects into account.

DOI: 10.1103/PhysRevB.65.214422 PACS number(s): 75.30.Vn, 75.30.Ds, 76.50.+g

## I. INTRODUCTION

The main physical properties of doped manganites were investigated nearly half a century ago by Jonker and van Santen[1] and Wollan and Koehler.[2] The observed doping and temperature dependences were qualitatively explained by de Gennes[3] using an interplay of Mn-O-Mn superexchange and Zener's double-exchange (DE) mechanism.[4] In this model, upon increasing doping the antiferromagnetic (AFM) and insulating (*I*) $LaMnO_3$ passes through a canted AFM (CAF) ground state and arrives at ferromagnetic (FM) and metallic (*M*) states at doping levels $x \gtrsim 0.2$. Within this picture a phase diagram of manganites has been constructed, which was in agreement with the existing experimental data.

The interest in doped manganites was considerably renewed after several groups observed exceptionally high values of the magnetoresistance in thin films,[5] later termed as ''colossal magnetoresistance'' (CMR). CMR effects at the ferromagnetic phase transition were analyzed within an extended double-exchange model,[6] but also with models taking a strong electron-phonon coupling[7,8] or a percolative metal-insulator transition[9] into account. Subsequently it was realized that the rich phase diagram observed in various manganite systems can only be explained by considering additional degrees of freedom such as Jahn-Teller distortions,[7,8] electronic correlations, and charge and orbital order.[10–13]

In this paper we present high-field electron-spin-resonance (ESR) investigations of single crystals of $La_{1-x}Sr_xMnO_3$ for concentrations $0 \leqslant x \leqslant 0.175$, ranging from the AFM insulator to the FM metallic regime. The paper is organized as follows. Section II discusses the problem of phase separation in manganites. The discussion is focused on the low-doping region of the phase diagram, where important information can be extracted from the high-field ESR experiments.[14,15] Section III presents the details of the sample preparation and the experimental procedure. The experimental results are discussed and presented within three groups: $0 \leqslant x < 0.1$, $0.1 \leqslant x \leqslant 0.15$, and $x > 0.15$, respectively. The first region can be well described as antiferromagnetic insulator with a (modulated) canted structure followed by a ferromagnetic insulating ground state and, finally, by the ferromagnetic metal for $x > 0.15$.

## II. PHASE SEPARATION VS CANTED STRUCTURE

Enormous theoretical and experimental efforts have been devoted to the problem of phase separation (PS) in manganites. Already Wollan and Koehler[2] have observed the coexistence of ferromagnetic and antiferromagnetic lines in the neutron-scattering spectra, an effect which could be equally explained by the canting of the parent antiferromagnetic structure or by phase separation into ferromagnetic and antiferromagnetic domains. Later on, de Gennes theoretically[3] derived the canted antiferromagnetic structure as a ground state of low-doped manganites. Since then a number of subsequent experimental results have been explained using the concept of a canted structure.[16–22]

However, in recent years a number of theoretical models predicted that the CAF structure becomes unstable against electronic phase separation into FM and AFM regions.[9,23–25] According to the calculations on the basis of different models, the phase separation is energetically favorable in the

 

whole range of the phase diagram. At present a number of reviews devoted especially to this problem is available in the literature.[26,27]

Phase diagrams of doped manganites are very complex and in many cases difficult to interpret. It is therefore reasonable to expect that different physical mechanisms play a major role at different parts of the phase diagram and the answer to the PS-CAF question will be ambiguous. Postponing for a moment the discussion of the experimental data, the situation is not simple even from the theoretical point of view. For example, analyzing lattice effects on the magnetism of $LaMnO_3$ using the local-spin-density approximation, Solovyev *et al.*[28] found a stable canted phase. Investigating the phase diagram of manganites on the basis of the DE model, Nagaev[24] confirmed the conclusions of de Gennes[3]: the CAF structure can be energetically favorable for certain portions of the phase diagram. Parameter regions resulting in a stable CAF phase have also been found using a Schwinger-boson representation for the magnetic moments.[29] More recently, similar results have been obtained reinvestigating the DE theory within either multiple-scattering theory[30] or within a model including Coulomb repulsion and electron-phonon coupling.[31] However, we recall that the stability of a CAF phase in manganites has been obtained by a comparative minority of theoretical concepts dedicated to the topic of phase separation.

A large body of experimental work has been devoted to the detection of phase separation in manganites, which led in many cases to convincing experimental evidence,[32,33] especially in the vicinity of the ferromagnetic phase transition.[34,35] The discussion of most of these results was recently reviewed by Dagotto *et al.*[26] In spite of enormous experimental progress in the field of phase separation, the region of low-doped $LaMnO_3$, and especially the composition range $x<0.1$ still remains to be the matter of discussion. Among others, the Sr- and Ca-doped $LaMnO_3$ represent the most extensively studied systems. Their physical properties are quite similar, especially in the low-doping regime. One of the most prominent differences is a slightly stronger effect of Sr substitution: the transition to a ferromagnetic insulator takes place around $x\simeq 0.1$ for Sr,[36,37] compared to $x\simeq 0.125$ for Ca-substitution.[38,39]

First neutron-scattering data measured on Ca-doped $LaMnO_3$ by Wollan and Koehler[2] have been interpreted as equally compatible with either the PS or CAF picture in the low-doped region. About 40 years later, after the interest to manganites has been renewed, Kawano *et al.*[18] explained the neutron-scattering and magnetization results as pointing towards the CAF magnetic structure. Later on, using the same technique, Hennion *et al.*[17,40] found evidence for inhomogeneities in the canted structure, which were termed ''magnetic droplets'' or ''magnetic polarons.'' It should be pointed out that these results have been interpreted using the CAF phase as a ground state with the droplets arising from the effective modulation of the canting angle. This picture of the modulated CAF phase was later confirmed by the same group.[38,39] Almost simultaneously with the neutron-scattering data, evidence of inhomogeneities in the low-doped region of the phase diagram were found by NMR spectroscopy by Allodi and co-workers.[41,42] The NMR spectra pointed toward pure phase segregation into FM and AFM domains (also see Refs. 43 and 44). The NMR results seemingly contradict other available experimental data on low-doped manganites, which point toward the CAF structure as the ground state. However, as discussed by Kumagai *et al.*,[43] the NMR spectra might be affected by the ceramic character of the samples. This open problem certainly deserves additional investigations.

The antiferromagnetic-resonance (AFMR) technique has been applied to Sr-doped $LaMnO_3$ in the low-doping regime ($0\leqslant x\leqslant 0.1$) without magnetic field by Mukhin *et al.*[14] In addition, these investigations have been carried out in magnetic fields on untwinned single crystals of $La_{1-x}Sr_xMnO_3$ with $x=0.05$.[15] Two resonance modes have been observed in the spectra, which revealed distinct excitation conditions, magnetic fields, and doping dependences. These results could be directly explained using the CAF picture, and have been found to contradict the phase separation into pure FM and AFM phases. In agreement with this conclusion, recent calculations of the spin-wave branches by Román and Soto[45] confirm the distinctive character of the AFMR experiments on solving the PS-CAF problem. However, the AFMR experiments do not exclude a possible modulation of the canting angle, as found in neutron-scattering experiments.[38,39] A statistical modulation due to the randomly distributed Sr defects rather produces an additional broadening of the observed lines.[14,15]

The problem of phase separation was addressed from the point of view of magnetization data by Paraskevopoulos *et al.*[36] and Geck *et al.*[46] Although the magnetization measurements cannot, in a general case, distinguish between PS and CAF structures, the detailed analysis of the anisotropic magnetization[36] or hysteresis curves[46] did provide weighty arguments in favor of a CAF structure.

Concluding the discussion on the PS-CAF problem for low-doped manganites, we try to formulate the description of the magnetic structure for the low-doped manganites, which seems to be consistent with the majority of existing experimental data: The magnetic ground state is represented by a canted magnetic structure, which is statically modulated around an average value. Therefore, the term *modulated canted structure* seems to be appropriate in this case. Such an idea of local inhomogeneities of spin canting was already discussed by de Gennes.[3] Naively, in weakly doped manganites every doping atom could be considered as a center, which tends to locally increase the canting angle and thus to produce the modulation of the CAF structure. However, according to the neutron-scattering data,[38,40] the inhomogeneities in the magnetic structure are roughly one order of magnitude larger than the distance between the doping ions.

## III. EXPERIMENTAL DETAILS

Single crystals of $La_{1-x}Sr_xMnO_3$ were grown by the floating-zone method with radiation heating.[47] Raw $La_2O_3$, $SrCO_3$, and $Mn_3O_4$ chemicals of a high purity (not less 99.99%) were used for the preparation of ceramic rods. Some excess of $Mn_3O_4$ concentration ($\sim 0.5$ at. %) was used in order to compensate for a Mn loss due to the evaporation

from the melt in the floating-zone process. The initial synthesis of the composition was provided by annealing the mixed powder at about 1200 °C for 24 h. After pressing of feed rods they were sintered at 1350 °C for 24 h. Single crystals with concentrations of $x \leqslant 0.075$ were grown in an Ar atmosphere, while for $x > 0.075$ the samples were grown in air. The typical growth direction was [110]. In order to obtain crack-free crystals they were annealed at a temperature of about 1300 °C. X-ray powder-diffraction measurements revealed single-phase materials. Two-dimensional x-ray topography of the crystals indicated a twin structure of all samples, except for $x = 0.05$, which turned out to be twin free.

The temperature dependence of the dc resistivity of $La_{1-x}Sr_xMnO_3$ (Ref. 48) was measured utilizing a four-point technique, and quantitatively and qualitatively resembles the data known from the literature.[49,50] In addition, the submillimeter-wave properties[51] and magnetization[36,52] of these samples was investigated, and was published previously. Plane-parallel plates of approximately $8 \times 8 \times 1$ mm$^3$ have been cut from the crystals for the high-field ESR measurements.

For frequencies $40 \leqslant \nu \leqslant 700$ GHz (1.3–23 cm$^{-1}$) the high-field ESR spectra were recorded using a quasioptical technique utilizing backward-wave oscillators as coherent light sources.[53] Depending upon the transparency of the samples, two different types of experiments have been employed, i.e., transmission and reflection geometry. Using a similar technique, high-field ESR spectra of $Nd_{1-x}Ca_xMnO_3$ were recently investigated by Dupont *et al.*[54]

Within the transmission geometry the conventional quasioptical arrangement[53] is equipped with a superconducting split-coil magnet. The Mylar optical windows allow one to carry out transmission experiments in magnetic fields up to 8 T with the field parallel (Faraday geometry) as well as perpendicular (Voigt geometry) to the propagation of the electromagnetic beam.[55] The combination of both geometries is especially important investigating the ferromagnetically ordered samples, because in both cases different resonance conditions occur due to demagnetization fields. For a thin platelet and neglecting anisotropy fields the following expression for the ferromagnetic resonance frequencies $\omega_{FM}$ are obtained:

$$\omega_{FM} = \gamma\sqrt{(H + 4\pi M)H} \quad \text{Voigt geometry} \quad (H \| \text{to the platelet surface}), \tag{1}$$

$$\omega_{FM} = \gamma|H - 4\pi M| \quad \text{Faraday geometry} \quad (H \perp \text{to the platelet surface}), \tag{2}$$

where $\gamma$ is the gyromagnetic ratio, $H$ is the magnetic field, and $M$ is the magnetization. Equations (1) and (2) have been derived under the assumption that the platelet is oriented perpendicular to the quasioptical beam (i.e., normal incidence). Therefore, the resonance frequencies are shifted to higher frequencies for the Voigt geometry and to lower frequencies for the Faraday geometry.

The simplicity of the transmission geometry allows two different experimental modes: frequency-sweep and field-sweep runs. In the frequency-sweep mode the data can be collected even without magnetic field, which strongly simplifies the detection of weakly field-dependent modes. The frequency-dependent transmission spectra are analyzed using the Fresnel formulas for the transmittance $T = |t|^2$ of a plane-parallel sample (Voigt geometry)[56]:

$$t = \frac{(1 - r^2)t_1}{1 - r^2 t_1^2}, \quad \text{where} \tag{3}$$

$$r = \frac{\sqrt{\varepsilon/\mu} - 1}{\sqrt{\varepsilon/\mu} + 1} \quad \text{and} \quad t_1 = \exp(-2\pi i\sqrt{\varepsilon\mu}\, d/\lambda).$$

Here $r$ is is the reflection amplitude at the air-sample interface, $t_1$ is the "pure" transmission amplitude, $\varepsilon$ and $\mu$ are the (complex) dielectric permittivity and the magnetic permeability of the sample, respectively, $d$ is the sample thickness, and $\lambda$ is the radiation wavelength. This expression can also be applied for anisotropic crystals, if the incident radiation is polarized along the principal optical axes. For experiments in the Faraday geometry the transmission has to be determined using more complicated expressions, which strongly depend on the mutual orientation of the analyzer and polarizer and will be presented in a separate paper.

The relatively good transparency of the low-doped ($x < 0.1$) manganites in the submillimeter frequency range resulted in interference patterns due to internal reflections from the sample surface. The observation of these interferences allowed a calculation of the optical parameters of the sample without measuring the phase shift of the transmitted signal. The dispersion of the magnetic permeability has been taken into account, assuming a harmonic oscillator model for the complex magnetic permeability,

$$\mu^*(\nu) = \mu_1 + i\mu_2 = 1 + \frac{\Delta\mu\,\nu_0^2}{\nu_0^2 - \nu^2 + i\nu\delta}, \tag{4}$$

where $\nu_0$, $\Delta\mu$, and $\delta$ are the eigenfrequency, mode strength, and width of the resonance, respectively. In a good approximation the dielectric parameters of the sample ($\varepsilon^* = \varepsilon_1 + i\varepsilon_2$) behave regularly in the vicinity of the resonance frequency. Hence, frequency-sweep measurements allowed one to obtain absolute values of the parameters of the ESR-AFMR lines.

The reflection geometry has been utilized in a top-loading 16 T superconducting magnet. Typical quasioptical elements have been set up outside the magnet. A stainless-steel rod has been constructed to guide the beam inside the magnet, which was finally focused onto the sample by a Teflon lens. This arrangement did not allow us change the sample against the reference mirror, which hampered frequency-sweep experiments. In the reflection experiment with the top-loading magnet the sample surface is perpendicular to the static magnetic field and to the propagation direction of the beam,

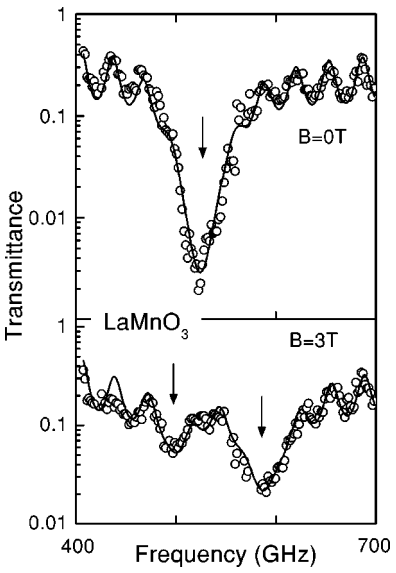


FIG. 1. Antiferromagnetic resonance observed in $LaMnO_3$ without magnetic field (upper panel) and in a static field with $B=3$ T. Symbols, experiment; lines, calculations on the basis of the Fresnel equations.

which corresponds to the Faraday geometry. The ESR signal was amplified by a lock-in technique with field modulation. Hence a field derivation of the spectra is detected.

## IV. RESULTS AND DISCUSSION

Since the early phase diagrams[49,57] of low-doped manganites a number of additional details and corrections were provided.[18,58,59] On the basis of the samples investigated in this work, a similar phase diagram was presented, which has been constructed using conductivity and magnetization measurements.[36,48] Except for minor details and slightly different interpretations, this diagram agrees well with the established ones and also with the detailed phase diagram, published recently by Lui *et al.*[37] These phase diagrams will be referred to when discussing the results of the high-field ESR experiments.

### A. Parent antiferromagnet ($x=0$)

Figure 1 shows the frequency dependence of the transmittance of $LaMnO_3$ in the frequency range of the antiferromagnetic resonance. The spectra in a zero magnetic field are dominated by an intensive absorption line around 520 GHz, which represents the AFMR mode. The transmittance spectra can be well approximated using a Lorentzian shape [Eq. 4] for the resonance mode. The fringes on both sides of the resonance line arise due to the interference of the beam reflected from the opposite sides of the sample. The amplitude and the period of these fringes allow an independent determination of the dielectric parameters of the sample. The solid lines in Fig. 1 represent the calculated transmittance of a plane-parallel sample according to the Fresnel equations [see Eq. (3)].

A better description of the resonance minimum can be achieved by assuming two closely separated AFMR lines instead of a single line.[14] Previously, the small splitting of the AFMR line was explained by the magnetic anisotropy due to the low (orthorhombic) symmetry of the crystal.[14] However, it is not clear at present whether this effect is simply due to a slight oxygen nonstoichiometry. The existence of a small canting was observed even in pure stoichiometric $LaMnO_3$,[60] and later[61] attributed to a Dzyaloshinski-Moriya exchange coupling.

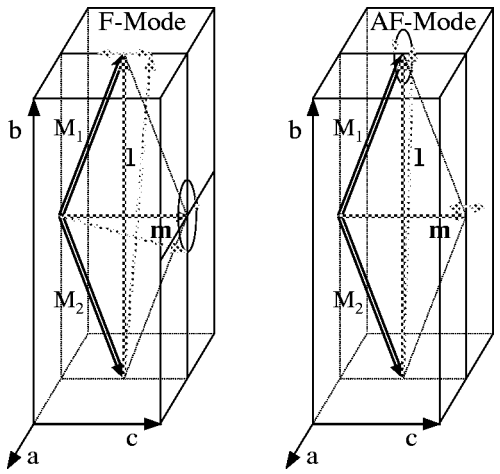


FIG. 2. Schematic representation of the antiferromagnetic modes for a canted antiferromagnetic structure. The magnetic moments of the two sublattices $\mathbf{M}_1$ and $\mathbf{M}_2$ correspond to adjacent *ab* layers, and are brought to the same point for simplicity. $\mathbf{m}=\mathbf{M}_1+\mathbf{M}_2$ is the ferromagnetic moment, and $\boldsymbol{l}=\mathbf{M}_1-\mathbf{M}_2$ is the antiferromagnetic moment. The oscillations corresponding to two possible modes are also shown (ellipses and double arrows). The quasiferromagnetic mode (*F*) is excited by $\tilde{h}\|a$ and $\tilde{h}\|b$, and the quasiantiferromagnetic mode (AF) is excited by $\tilde{h}\|c$.

The application of the static magnetic field splits the AFMR mode into two clearly resolved modes (lower frame of Fig. 1). This behavior is typical for an antiferromagnet,[62,63] and was previously observed in field-sweep spectra in pure $LaMnO_3$ by Mitsudo *et al.*[64] Within a simplified picture the line splitting takes place for the orientation of the external magnetic field parallel to the magnetic moments of the sublattices (i.e., parallel to the antiferromagnetic vector, $l=\mathbf{M}_1-\mathbf{M}_2$, in Fig. 2). For a two-sublattice axial antiferromagnet the external magnetic field along the easy axis removes the degeneracy of two circularly polarized modes and splits them into two lines. The corresponding resonance frequencies $\omega_\pm$ are given in a crude approximation simply by[62]

$$\omega_\pm=\omega_0\pm\gamma H. \tag{5}$$

Here $\omega_0$ is the resonance frequency without an external field, $H$ is the magnetic field parallel to the antiferromagnetic vector, and $\gamma$ is the gyromagnetic ratio. A closer analysis of the field-dependent antiferromagnetic resonances in Fig. 1 reveals the appearance of an additional splitting of the lines, which is due to twinning of the crystal and is documented in Fig. 10 (Sec. V).

### B. Canted antiferromagnet ($0<x<0.1$)

As discussed in Sec. II, as far as low-doped manganites are concerned, the concept of a (modulated) canted magnetic structure is in good agreement with the majority of experimental data in the field.[2,14–22,36–40,46,49,52] Specifically for the high-field ESR experiments, this concept successfully describes the splitting of the antiferromagnetic lines, excitation conditions, magnetic-field dependence, doping dependence, etc.[14,15] To our best knowledge there exists no theory which could explain the AFMR data on the basis of phase separation into pure FM and AFM regions. Therefore, the following presentation and discussion will be given within the concept of the canted magnetic structure only.

The substitution of the trivalent $La^{3+}$ in the parent $LaMnO_3$ by divalent $Sr^{2+}$ or $Ca^{2+}$ introduces holes in the structure. Assuming Zener's double-exchange mechanism,[3,4] the holes favor the ferromagnetic orientation of the magnetic lattice, and therefore lead to a canting of the magnetic moments along the crystallographic $c$ axis.

Compared to the pure antiferromagnetic structure, the modes of the antiferromagnetic resonance are split even in the absence of an external magnetic field. The resonances of the canted structure can be well described by separating two sublattices of both magnetization directions ($\mathbf{M}_1$ and $\mathbf{M}_2$, the two-sublattice model[65]). The behavior of the antiferromagnetic resonances of the canted structure was calculated by a number of authors,[65–67] and especially for manganites by de Gennes[3] nearly 40 years ago.

The two modes observed can be represented as the oscillations of the ferromagnetic and antiferromagnetic vectors, $\mathbf{m}=\mathbf{M}_1+\mathbf{M}_2$ and $\boldsymbol{l}=\mathbf{M}_1-\mathbf{M}_2$, respectively. Here $\mathbf{M}_1$ and $\mathbf{M}_2$ are the magnetizations of the sublattices. These vectors and the corresponding modes are represented in Fig. 2. The two AFMR modes can be termed quasiferromagnetic ($F$ mode) and quasiantiferromagnetic (AF mode) resonances, respectively. The interaction of the modes with the electromagnetic field is realized via the term $(\mathbf{m}\cdot H)$ in the free energy. The oscillations in the $F$ mode involve the following components of the magnetic vectors: $\mathbf{m}_a, \mathbf{m}_b$, and $\boldsymbol{l}_c$ (Fig. 2, left panel). This mode can therefore be excited by the electromagnetic wave with the ac magnetic field $(\tilde{h})$ having a nonzero component in the $ab$ plane. By analogy, the AF mode (Fig. 2, right panel), which involves $(\mathbf{m}_c, \boldsymbol{l}_a, \boldsymbol{l}_b)$ is excited for $(\tilde{h})$ lying along the $c$ axis.[66,68]

A realistic two-sublattice model for manganites[68] was successfully applied to the doping dependence of the AFMR-modes in $La_{1-x}Sr_xMnO_3$,[14] and to the magnetic-field dependence of the resonances in the untwinned $La_{0.95}Sr_{0.05}MnO_3$ single crystal.[15] An example of the transmittance spectra in the field-sweep modus for $x=0.05$ is given in Fig. 3, which represents the field dependence of the submillimeter transmittance for two different orientations. Above the antiferromagnetic transition $T_N \simeq 140$ K a single line of the electron-paramagnetic resonance (EPR) at $g \simeq 2$ is observed. The width of the EPR line for $\tilde{h} \| c$ ($B \| b$, upper panel) is substantially larger than the linewidth for $\tilde{h} \| b$ ($B \| c$, lower panel). Below the magnetic ordering transition the mode with $\tilde{h} \| b$

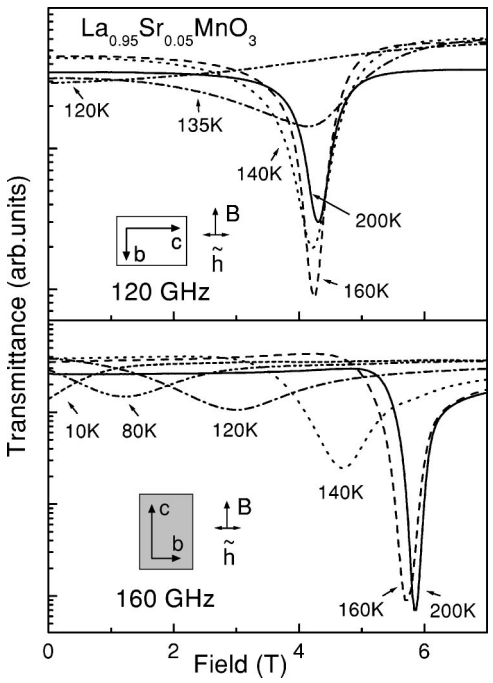


FIG. 3. High-field ESR spectra of an untwinned $La_{0.95}Sr_{0.05}MnO_3$ single crystal for two experimental geometries, as indicated, and for temperatures below and above $T_N \simeq 140$ K.

(lower panel of Fig. 3) rapidly shifts to lower fields, and finally stabilizes at $\sim 180$ GHz at low temperature and in zero magnetic field. According to the excitation conditions and the zero-field resonance frequency, this mode corresponds to the quasiferromagnetic mode in Fig. 2.

The resonance line in the upper panel of Fig. 3 apparently disappears below the magnetic transition. However, the analysis of the high-frequency spectra shows that this line strongly broadens in the field-sweep scale. Similar to the quasi-$F$ mode, this line shifts to lower fields and saturates at $\nu \sim 420$ GHz (for $B=0$ T). The large difference between this value and the frequency of the field-sweep experiment (120 GHz) is the second reason for the apparent disappearance of the ESR line as documented in the upper panel of Fig. 3.

Figure 4 shows the temperature dependence of the parameters of the ESR modes of Fig. 3. These data have been obtained mainly from the analysis of the frequency-dependent transmittance via Eqs. (3) and (4). As demonstrated in the lower panel of Fig. 4, in the paramagnetic state the ESR line is located around $g \simeq 2$, independent of the orientation of the magnetic field. In the magnetically ordered state the excitation conditions become orientation selective (Fig. 2), and both geometries reveal strongly different resonance frequencies. In addition, the lower panel of Fig. 4 reveals that the magnetic-field-induced shift of the ordering temperature is also orientation dependent. The corresponding transition temperatures are marked by $T_N=T_1$ and $T_2$, respectively. The magnetic field along the $c$ axis favors the low-temperature magnetic configuration $\mathbf{m} \| c$, $\boldsymbol{l} \| b$, and therefore strongly enhances $T_N=T_2$. Conversely, for $B \| b$ the application of the static field favors the configuration $\mathbf{m} \| b, \boldsymbol{l} \| c$,

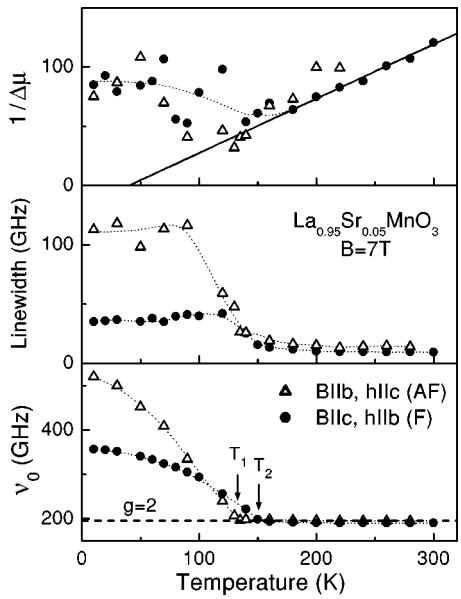


FIG. 4. Temperature dependence of the parameters of the ESR modes in $La_{0.95}Sr_{0.05}MnO_3$. The parameters have been obtained analyzing the frequency-dependent transmittance as described in the text. The symbol notation is the same in all frames. The experimental geometry corresponds to that of Fig. 3. Dotted lines are guides to the eye. Upper panel: Inverse line intensity. The solid line for $B||c$ corresponds to a Curie-Weiss law with $\mu_{\text{eff}} \simeq 7\mu_B$. Middle panel: Linewidth. Lower panel: Resonance frequency. The dashed line indicates $g=2$. Arrows mark different Néel temperatures for the two measuring geometries.

which is energetically unstable. In that case the transition at $T_N = T_1$ broadens and remains approximately field-independent.

As is documented in the middle panel of Fig. 4, the ESR line strongly broadens below $T_N \simeq 140$ K. This explains the nonobservability of these lines in conventional *X*-band ESR,[69] and the apparent disappearance of the $B||b$ mode in the upper panel of Fig. 3. The anisotropy of the linewidth at low temperatures is seen both in the paramagnetic and in the magnetically ordered state. From an extensive analysis of *X*-band (9 GHz) ESR experiments,[69,70] this anisotropy has been attributed to the Dzyaloshinski-Moriya interaction and to the crystal-field effects. A detailed report on the low-frequency EPR experiments in $La_{1-x}Sr_xMnO_3$ was published elsewhere.[69,70]

The upper panel of Fig. 4 shows the mode contribution of the ESR modes in $La_{0.95}Sr_{0.05}MnO_3$. The contributions of both modes coincide within the experimental accuracy. The absolute values of the contribution ($\Delta\mu \sim 0.01$) agree well with the predictions of the two-sublattice model.[15] The mode contribution for $B||c$ in the paramagnetic state follows a Curie-Weiss behavior. However, the estimate of the effective paramagnetic moment yields $\mu_{\text{eff}} \simeq 7\mu_B$, which is substantially higher than $\mu_{\text{eff}} \simeq 5.5\mu_B$, obtained from the dc susceptibility.[36] This effect most probably is due to the smearing of the Curie-Weiss law in the vicinity of the Neél temperature and in high magnetic fields ($B = 7$ T).

A detailed analysis of the AFMR modes in $La_{0.95}Sr_{0.05}MnO_3$ and at low temperatures was published previously.[15] In agreement with the classical predictions for a canted antiferromagnet, two AFMR lines could be observed, which revealed distinct excitation conditions and magnetic-field dependence. The full set of the experimental data including the magnetization and AFMR modes was satisfactorily explained using a two-sublattice model of the canted magnetic structure.

A qualitatively similar behavior was also observed for $La_{0.925}Sr_{0.075}MnO_3$. However, this sample turned out to be heavily twinned and the separation of the different orientations was not possible. As will be shown below (Fig. 10, Sec. V), the field dependence of the antiferromagnetic resonances is again well described by the two-sublattice model of the canted structure.

### C. Ferromagnetic insulator ($0.10 \leqslant x \leqslant 0.15$)

The doping dependence of the AFMR frequencies in the low-*x* region of the phase diagram, which has been discussed in the previous sections, reveals a gradual softening of the quasiferromagnetic mode and a weakening of the quasiantiferromagnetic mode (Fig. 2). In de Gennes' scenario a ferromagnetic and metallic phase follows the CAF structure. In manganites an intermediate ferromagnetic insulating state is found for Sr and Ca doping. This FM/I state most probably results from a suppression of the static Jahn-Teller distortions, the increasing importance of the orbital degeneracy and a subsequent onset of a new orbital order which stabilizes the ferromagnetic insulator. In the ferromagnetic state demagnetization effects due to the spontaneous magnetization start to become important. In addition, the insulating character of the manganites in this composition range leads to additional complications of the spectra.

Figures 5 and 6 show the high-field ESR spectra of $La_{1-x}Sr_xMnO_3$ with $x = 0.125$ measured in Faraday geometry. Compared to the spectra of the lower-doped manganites, these data are more difficult to interpret. We recall that in this concentration range $La_{1-x}Sr_xMnO_3$ is a ferromagnetic insulator, and that the spectra are expected to consist of a single ferromagnetic resonance (FMR) mode. The physical origin of the complicated spectra observed is due to additional electrodynamic effects, which arise in Faraday geometry and for high intensities of the FMR mode. In the Faraday geometry left- and right-rotating circular polarized components of the incident radiation reveal strongly different propagation constants near resonance. As a result, the linearly polarized incident wave transforms into an elliptically polarized wave. Depending on the relative orientation of the analyzer and polarizer, qualitatively different transmission (reflection) spectra are expected. Multiple reflections of the radiation within the platelet-shaped sample result in additional peculiarities. Similar effects in the vicinity of an AFMR mode were observed previously in the orthoferrite $YFeO_3$.[71]

Within the transmission geometry of our experiments the analyzer is positioned parallel to the polarizer. Taking into account the above-mentioned effects, we have simulated

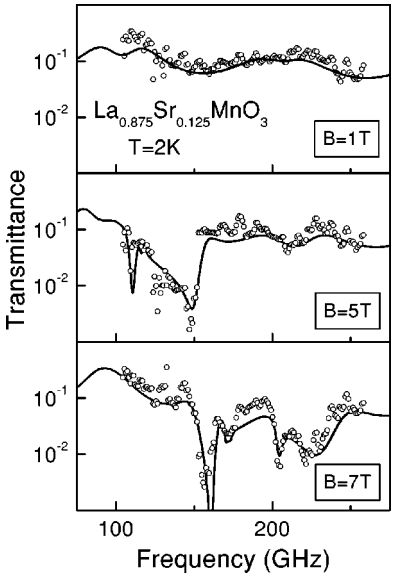


FIG. 5. Frequency-dependent transmittance of a 0.194-mm-thick $La_{0.875}Sr_{0.125}MnO_3$ single crystal in the Faraday geometry. Upper panel: $B=1$ T; the FMR mode is below the frequency range of the experiment. Middle ($B=5$ T) and lower ($B=7$ T) panels: the complicated character of the FMR spectra is due to interference effects and Faraday rotation. Symbols, experiment. The lines represent the calculated transmittance of the platelet-shaped sample assuming a parallel orientation of the polarizer and analyzer. The model parameters are the same for all curves: $g=2$, $M \simeq 4\mu_B$/Mg atom, $\varepsilon^* = 56 + i5.7$, FMR linewidth $\delta = 0.1$ cm$^{-1}$.

these spectra both for the frequency (Fig. 5) and field (Fig. 6) sweeping modes. A single ferromagnetic resonance mode [Eqs. (4) and (2)] has been taken into account using $g=2$ and a magnetic susceptibility characteristic for an ordinary ferromagnet. The FMR linewidth was used as the only fitting parameter ($\delta = 0.1$–$0.15$ cm$^{-1}$), since the intensity and the frequency shift of the FMR mode are directly determined by the magnetization, which was taken from static measurements ($M \simeq 4\ \mu_B$/Mn atom[36,52]). The complex dielectric permittivity, which is also important to explain these phenomena, was determined by fits of the transmittance at $H=0$ as $\varepsilon^* = 56 + i5.7$. No further fitting parameters have been utilized. The reasonable agreement between theory and experiment demonstrates the validity of our ansatz using a single FMR mode. Similar transmittance spectra were also observed for the composition $x=0.1$ (not shown), which revealed even more pronounced peculiarities in a thicker sample. Finally, we note that in some sense the observed anomalies of the transmission spectra can be considered as magnetostatic modes.[72]

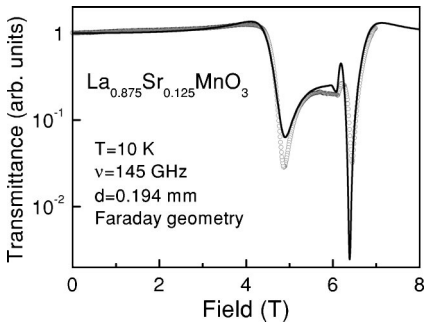


FIG. 6. High-field ESR spectra of $La_{0.875}Sr_{0.125}MnO_3$ in the Faraday/transmission geometry. Symbols, experiment; line, theory, which takes into account only a single ferromagnetic resonance mode and electrodynamic effects in the Faraday geometry (see the text). The model parameters are the same as given in Fig. 5.

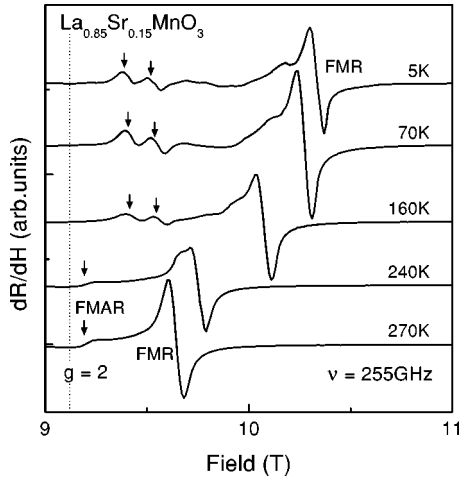


FIG. 7. High-field ESR spectra of $La_{0.85}Sr_{0.15}MnO_3$ in the Faraday/reflection geometry revealing ferromagnetic resonance and antiresonance modes. The curves are shifted for clarity. The antiresonance modes are marked by arrows. The line splitting results from the residual influence of the electrodynamic effects (magnetostatic modes).

Closer to the ferromagnetic metallic region of the phase diagram ($x \gtrsim 0.15$) the increase of the conductivity hampers the transmission experiments. Therefore, in this composition range the reflectance geometry has been employed in our high-field ESR experiments. A typical example of a field-sweep curve is represented in Fig. 7, showing ESR spectra of $La_{0.85}Sr_{0.15}MnO_3$. We recall that the reflection experiments have been carried out within the Faraday geometry. The spectra in Fig. 7 are dominated by the single ferromagnetic resonance, which is shifted to higher magnetic fields by the value of the static magnetization [cf. Eq. (2)]. Due to only weak interference effects in reflection measurements of thick samples, the line of the ferromagnetic *antiresonance* (FMAR) (Ref. 73) becomes clearly visible, and is indicated by arrows.

A FMAR line has previously been observed in manganites[74–76] as a minimum in the microwave absorption. The FMAR line corresponds to the zero crossing of the real part of the magnetic permeability $[\mu^*(\omega,B) = \mu_1 + i\mu_2]$, which leads to a *minimum* in the reflectance. Therefore, in the field derivative ($dR/dH$) this line reveals an opposite sign, compared to the FMR mode, which corresponds to a local *maximum* in reflectance.

Figure 8 shows the temperature dependence of the high-field ESR modes for $La_{0.9}Sr_{0.1}MnO_3$ and $La_{0.85}Sr_{0.15}MnO_3$. The complicated pattern observed for $x=0.1$ and shown in the upper panel is related to the above-discussed interference effects near the ferromagnetic resonance. The temperature

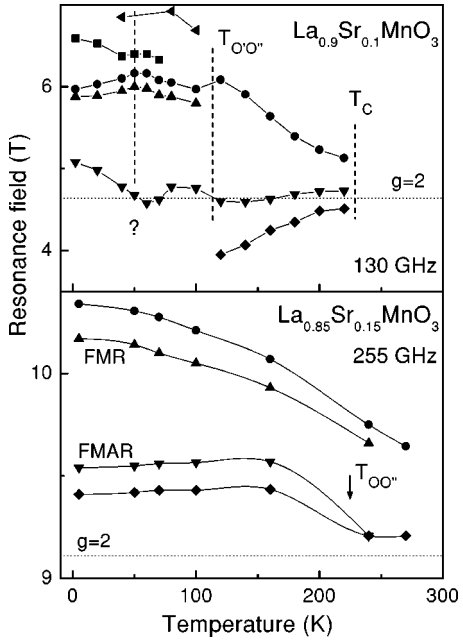


FIG. 8. Temperature dependence of the ESR modes in the Faraday geometry. Solid lines are drawn to guide the eye. Symbols represent different observed modes. Dotted lines indicate $g=2$. Upper panel: $La_{0.9}Sr_{0.1}MnO_3$. Dashed lines mark the phase-transition temperatures. Lower panel: $La_{0.85}Sr_{0.15}MnO_3$.

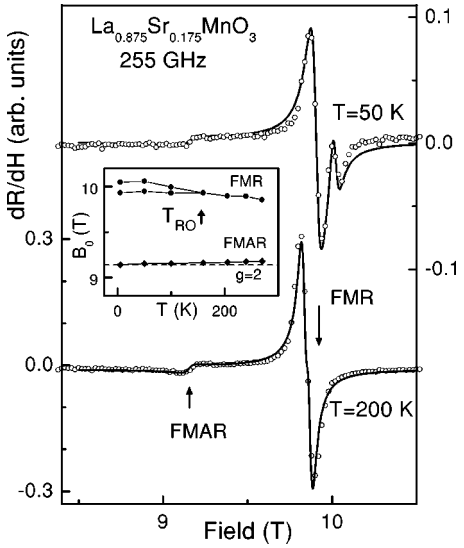


FIG. 9. High-field ESR spectra of $La_{0.825}Sr_{0.175}MnO_3$ in the Faraday/reflection geometry. The ferromagnetic resonance and antiresonance modes are marked by arrows. Symbols, experiment; lines, fit. The line splitting of the FMR mode is due to the anisotropy of the crystal field below the rhombohedral-to-orthorhombic phase transition at $T_{RO}$. The inset shows the temperature dependence of the resonance-line positions.

dependence of the line positions reflects the change of the magnetization and of the dielectric permittivity. The number of modes becomes reduced for higher temperatures, i.e., as the sample becomes closer to paramagnetic state where gyrotropic and interference effects are much weaker. The data in the upper panel of Fig. 8 correspond to a static magnetic field of 5–6 T. This is most probably the reason why the magnetic ordering near 210 K becomes rather smooth and is shifted by about 60 K compared to $T_C \simeq 150$ K observed at zero magnetic field. Conversely, the transition to the orbital-ordered state $T_{O'O''} \simeq 120$ K is only weakly affected by the magnetic field. In addition to these well-known transitions, the temperature dependence of the ESR lines reveals an anomaly around 60 K. The nature of this transition is not clear at present. In this context we would like to mention the recent observation[77] of anomalies in the thermal conductivity of $La_{0.9}Sr_{0.1}MnO_3$ around $T_{LO} \simeq 75$ K, which may correspond to the anomalies in the high-field ESR spectra, observed around $T=60$ K.

The lower panel of Fig. 8 shows the temperature dependence of the FMR and FMAR modes of $La_{0.85}Sr_{0.15}MnO_3$. The increase of the FMAR frequency below $\sim 210$ K could be related to an increase of the anisotropy field below the structural $OO''$ transition, which has been observed in $La_{0.9}Sr_{0.1}MnO_3$ (Ref. 75) and $La_{0.8}Sr_{0.2}MnO_3$ (Ref. 76) by magnetic resonance studing at low frequencies. The observed line splitting is probably due to interference effects, to different $g$ factors for nonequivalent Mn sites, and to the sample twinning. The frequency of the ESR experiment approximately corresponds to a static magnetic field of 10 T. Such a high field smears the magnetic-ordering transition and strongly increases the transition temperature for $La_{0.85}Sr_{0.15}MnO_3$, which can be estimated as $T_C \simeq 350$ K. This corresponds to a shift of 130 K compared to the zero-field value of $T_C \simeq 220$ K.[36]

### D. Ferromagnetic metal, $x=0.175$

For $x \geqslant 0.15$ the conductivity of $La_{1-x}Sr_xMnO_3$ rapidly increases, resulting in a significant increase of the absolute reflectivity. Typical high-field ESR spectra in this composition range are represented in Fig. 9. As observed in $La_{0.85}Sr_{0.15}MnO_3$, the spectra obtained in $La_{0.825}Sr_{0.175}MnO_3$ show two lines of opposite sign, which correspond to FMR and FMAR modes. Because $La_{0.825}Sr_{0.175}MnO_3$ is already in a ferromagnetic state at all temperatures investigated, both lines reveal no substantial temperature dependence. The intensity of these lines decreases for decreasing temperature. This effect is easily explained by the increase of the conductivity toward low temperatures, and, consequently, by the increase of the absolute reflectance. In this case the relative effect of the magnetic resonance line decreases. Assuming a temperature independent contribution of the FMR mode the simulation of the line intensity yields a value of the dc resistivity, $\rho_{dc} = 1/\sigma_1 \sim 10^{-4}\Omega$ cm at low temperature, which is in agreement with the measured value.[48]

At low temperatures the line of the ferromagnetic resonance becomes split. The analysis of the temperature dependence of the splitting (inset of Fig. 9) shows that the splitting starts at the rhombohedral-to-orthorhombic ($R/O$) transition.[36,37,48] Using the temperature-dependent powder x-ray spectroscopy, the $R/O$ transition temperature has been determined as $T_{RO} \simeq 180$ K for this sample. Therefore, we attribute the splitting of the FMR line to the increase of the

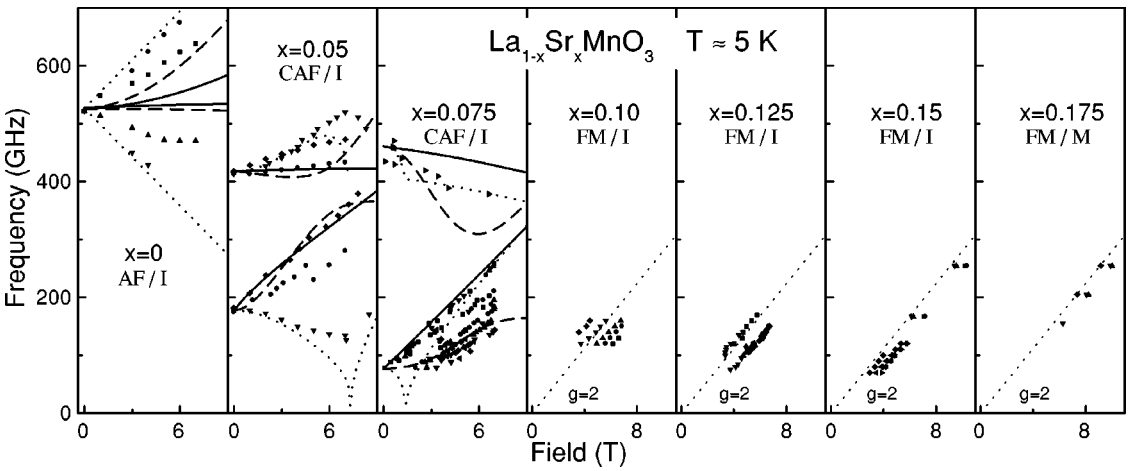


FIG. 10. Summary of the high-field ESR spectra of $La_{1-x}Sr_xMnO_3$ at low temperatures. AF, antiferromagnet; CAF, canted AF; FM, ferromagnet, *I*, insulator; *M*, metal. Symbols, experiment. Lines for $x \leqslant 0.075$ represent the model for the canted magnetic structure and the $g=2$, position for $x \geqslant 0.1$. The sample orientation and excitation conditions are determined unambiguously for the $x=0.05$ concentration only (see Ref. 15 for details). The data for $x \geqslant 0.1$ have been obtained in the Faraday geometry.

crystal anisotropy at the $R/O$ transition. (The simultaneous observation of two lines arises from the twinning of the sample.) This effect is directly connected to lowering of the crystal symmetry below $T_{RO}$. In principle, one could expect a similar splitting for the FMR lines for $0.1 \leqslant x \leqslant 0.15$, which are all in the orthorhombically distorted phase ($O''$). But this effect is probably masked by the larger linewidth for these concentrations. We note that the interference effects are not excluded completely, even for the highly conducting $La_{0.825}Sr_{0.175}MnO_3$.

## V. SUMMARY

Figure 10 summarizes the high-field ESR results in $La_{1-x}Sr_xMnO_3$ for all compositions investigated. The parent compound $LaMnO_3$ is purely antiferromagnetic and reveals two nearly degenerate AFMR lines ($x=0$). These lines become split in an external magnetic field, as is expected for a conventional antiferromagnet.

In the lowest-doping regime $0 \leqslant x \leqslant 0.075$ the compounds reveal close similarities concerning the appearance and the splitting of the AFMR modes. Already without a magnetic field for increasing Sr concentration, the initially degenerate AFMR modes split into quasiferromagnetic ($F$) and quasiantiferromagnetic (AF) modes. The $F$ mode rapidly softens and finally transforms into the line of ferromagnetic resonance for $x \geqslant 0.09$. The AF mode reveals a much weaker composition dependence and disappears in the ferromagnetic state. The lines in Fig. 10 for $0 \leqslant x \leqslant 0.075$ represent the calculations using a two-sublattice model of the canted magnetic structure (Sec. IV B). Figure 10 shows the results for all orientations of the magnetic field simultaneously. For $x=0$ and 0.075 this cannot be avoided because of the twinning of the samples. For $x=0.05$ the comparison between theory and experiment can be carried out for all orientations separately (see Ref. 15 for a detailed analysis). Taking into account the twinning of the crystals, the two-sublattice model of the canted magnetic structure can well reproduce the high-field EPR spectra of the low-doped $La_{1-x}Sr_xMnO_3$ compounds.

The composition range $0.1 \leqslant x \leqslant 0.15$ corresponds to the ferromagnetic insulator at low temperatures. The ESR spectra in this concentration range are rather complicated, which can be attributed to the interference of two normal modes (right- and left-circular polarizations) near the ferromagnetic resonance, resulting in a significant change of the polarization of the incident radiation. The spectra in Fig. 10 are shown for the Faraday geometry, and are therefore shifted to higher fields compared to $g=2$ (dashed lines for $0.1 \leqslant x \leqslant 0.175$). All data can be satisfactorily accounted for using a *single* FMR mode.

The high-field ESR spectra for higher doping levels show ferromagnetic resonance (FMR) and ferromagnetic antiresonance (FMAR) modes. In addition, a splitting of the FMR mode is observed in $La_{0.825}Sr_{0.175}MnO_3$ below the structural orthorhombic/rhombohedral transition which is attributed to a lowering of the crystal symmetry.

Finally, we would like to compare the gap value of the spin-wave branches as determined in the present work with those as derived from neutron-scattering experiments in Sr-doped manganites. The wavelength of the submillimeter radiation is much larger than the interatomic distance. Therefore, the high-field ESR determines the gap values at the center of the Brillouin zone. The concentration dependencies of the high-frequency (QAF) and low-frequency (QF) mode are shown in Fig. 11 as determined at $T \simeq 5$ K.

The high-field ESR results agree well with the neutron-scattering data for $La_{0.94}Sr_{0.06}MnO_3$,[38] which are included in Fig. 11 for comparison. A similar concentration dependence of the spin gap was obtained in Ca-doped manganites.[39] For $0.025 \leqslant x \leqslant 0.1$ the concentration behavior of the quasiferromagnetic branch is approximately linear. Conversely, the quasiantiferromagnetic mode is roughly constant in this concentration range. At $x \simeq 0.1$ the low-frequency branch becomes zero and the high-frequency mode disappears. This behavior corresponds well to the transition from the CAF to the ferromagnetic state with a gapless spin-wave branch. A

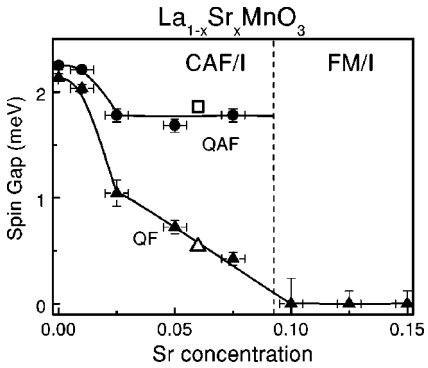


FIG. 11. Doping dependence of the spin gap in $La_{1-x}Sr_xMnO_3$ from AFMR (Ref. 14) and high-field ESR experiments. Closed circles, quasiantiferromagnetic (QAF) mode; closed triangles, quasiferromagnetic (QF) mode (see Sec. IV B for details). Open symbols represent the neutron-scattering results (Ref. 38). Note the disappearance of the QAF branch at $x \sim 0.1$. The unusual doping dependence around $x \sim 0.025$ reflects a possible threshold concentration between the antiferromagnetic and canted structures.

very small nonzero gap ($\nu_0 \sim 0.019$ meV) was observed in $La_{0.85}Sr_{0.15}MnO_3$ in inelastic neutron-scattering experiments.[78] However, this value cannot be distinguished from zero within the accuracy of our experiment. Nevertheless, the splitting of the FMR line for $x = 0.175$ is of comparable amplitude ($0.12\ \mathrm{T} \hat{=} 0.014$ meV). Finally, we note that for $x \geqslant 0.1$ a FM ground state with a different orbital order is established.

An unusual behavior of the AFMR frequencies is observed for low concentrations (Fig. 11). For $x \leqslant 0.025$ both modes are close to each other, and approximately independent of doping. We suggest that this may reflect the stability of the pure antiferromagnetic state against canting for low doping concentration. Above a threshold value of $x \simeq 0.025$ the doping by $Sr^{2+}$ leads to the abrupt increase of the canting angle and to the corresponding drop of the AFMR frequencies. We note that such a transition above some critical concentration was predicted theoretically by several authors.[79]

In conclusion, using the high-field ESR technique we have investigated the magnetic properties of $La_{1-x}Sr_xMnO_3$ for compositions ranging from the antiferromagnetic insulator to the ferromagnetic metal. In undoped $LaMnO_3$ a splitting of the antiferromagnetic resonance mode is observed only in the external magnetic field, in agreement with the antiferromagnetic structure of this material. For increasing Sr doping the AFMR modes are split even in zero field, which can be naturally explained assuming a canted magnetic structure for $x < 0.1$. A possible threshold concentration from the antiferromagnetic to the canted state is observed around $x \simeq 0.025$. In the ferromagnetic insulating state ($0.1 \leqslant x \leqslant 0.15$) a complicated set of spectra has been observed. However, these spectra can be well explained by a single ferromagnetic resonance mode and taking into account electrodynamic effects. In $La_{0.825}Sr_{0.175}MnO_3$ the ESR spectra are consistent with the ferromagnetic and metallic state. The lines of ferromagnetic resonance and ferromagnetic antiresonance can be clearly observed in reflectance geometry. Therefore, the ground state of $La_{1-x}Sr_xMnO_3$ for $x \leqslant 0.175$ can be well characterized by high-field ESR techniques.

## ACKNOWLEDGMENTS

We acknowledge stimulating discussion with M. Hennion, D. Khomski, J. Deisenhofer, and M. Paraskevopoulos. We are indebted to M. Müller, A. Pimenova, and F. Mayr for carrying out SQUID and x-ray experiments. This work was supported in part by BMBF (13N6917/0 - EKM), by DFG (SFB 484), by INTAS (97-30850) and RFBR (99-02-16848).

*Corresponding author. Email address:
Andrei.Pimenov@Physik.Uni-Augsburg.DE

[1] G.H. Jonker and J.H. van Santen, Physica (Amsterdam) **16**, 337 (1950); **19**, 120 (1953).
[2] E.O. Wollan and W.C. Koehler, Phys. Rev. **100**, 545 (1955).
[3] P.-G. de Gennes, Phys. Rev. **118**, 141 (1960).
[4] C. Zener, Phys. Rev. **82**, 403 (1951).
[5] K. Chahara, T. Ohno, M. Kasai, and Y. Kozono, Appl. Phys. Lett. **63**, 1990 (1993); R. von Helmolt, J. Wecker, B. Holzapfel, L. Schultz, and K. Samwer, Phys. Rev. Lett. **71**, 2331 (1993); S. Jin, T.H. Tiefel, M. McCormack, R.A. Fastnacht, R. Ramesh, and L.H. Chen, Science **264**, 413 (1994).
[6] N. Furukawa, J. Phys. Soc. Jpn. **63**, 3214 (1994).
[7] A.J. Millis, P.B. Littlewood, and B.I. Shraiman, Phys. Rev. Lett. **74**, 5144 (1995).
[8] H. Röder, Jun Zang, and A.R. Bishop, Phys. Rev. Lett. **76**, 1356 (1996).
[9] A. Moreo, S. Yunoki, and E. Dagotto, Science **283**, 2034 (1999); A. Moreo, M. Mayr, A. Feiguin, S. Yunoki, and E. Dagotto, Phys. Rev. Lett. **84**, 5568 (2000).
[10] R. Maezono, S. Ishihara, and N. Nagaosa, Phys. Rev. B **58**, 11 583 (1998).
[11] R. Kilian and G. Khaliullin, Phys. Rev. B **58**, 11 841 (1998).
[12] P. Horsch, J. Jaklič, and F. Mack, Phys. Rev. B **59**, 6217 (1999).
[13] J. van den Brink, P. Horsch, F. Mack, and A.M. Oleś, Phys. Rev. B **59**, 6795 (1999).
[14] A.A. Mukhin, V.Yu. Ivanov, V.D. Travkin, A. Pimenov, A. Loidl, and A.M. Balbashov, Europhys. Lett. **49**, 514 (2000).
[15] A. Pimenov, M. Biberacher, D. Ivannikov, A. Loidl, V.Yu. Ivanov, A.A. Mukhin, and A.M. Balbashov, Phys. Rev. B **62**, 5685 (2000).
[16] Z. Jirák, S. Krupička, Z. Šimša, M. Dlouhá, and S. Vratislav, J. Magn. Magn. Mater. **53**, 153 (1985).
[17] M. Hennion, F. Moussa, J. Rodríguez-Carvajal, L. Pinsard, and A. Revcolevschi, Phys. Rev. B **56**, R497 (1997).
[18] H. Kawano, R. Kajimoto, M. Kubota, and H. Yoshizawa, Phys. Rev. B **53**, 2202 (1996); H. Kawano, R. Kajimoto, M. Kubota, and H. Yoshizawa, *ibid.* **53**, R14 709 (1996); H. Yoshizawa, H. Kawano, Y. Tomioka, and Y. Tokura, *ibid.* **52**, R13 145 (1995).
[19] A. Chakraborty, D. Bhattacharya, and H.S. Maiti, Phys. Rev. B **56**, 8828 (1997).
[20] Y. Okimoto, T. Katsufuji, T. Ishikawa, T. Arima, and Y. Tokura, Phys. Rev. B **55**, 4206 (1997).
[21] S. de Brion, F. Ciorcas, G. Chouteau, P. Lejay, P. Radaelli, and C.

Chaillout, Phys. Rev. B **59**, 1304 (1999).
[22] V. Skumryev, F. Ott, J.M.D. Coey, A. Anane, J.-P. Renard, L. Pinsard-Gaudart, and A. Revcolevschi, Eur. Phys. J. B **11**, 401 (1999).
[23] E.L. Nagaev, Usp. Fiz. Nauk. **166**, 833 (1996) [Sov. Phys. Usp. **39**, 781 (1996)].
[24] E.L. Nagaev, Phys. Rev. B **58**, 2415 (1998).
[25] S. Yunoki, J. Hu, A.L. Malvezzi, A. Moreo, N. Furukawa, and E. Dagotto, Phys. Rev. Lett. **80**, 845 (1998); S. Yunoki, A. Moreo, and E. Dagotto, *ibid.* **81**, 5612 (1998).
[26] E. Dagotto, T. Hotta, and A. Moreo, Phys. Rep. **344**, 1 (2001).
[27] M. Yu.Kagan and K.I. Kugel', Usp. Fiz. Nauk. **171**, 577 (2001) [Phys. Usp. **44**, 553 (2001)].
[28] I. Solovyev, N. Hamada, and K. Terakura, Phys. Rev. Lett. **76**, 4825 (1996).
[29] D.P. Arovas and F. Guinea, Phys. Rev. B **58**, 9150 (1998).
[30] I.V. Solovyev and K. Terakura, Phys. Rev. B **63**, 174425 (2001).
[31] L.-J. Zou, H.Q. Lin, and D.K. Campbell, Phys. Rev. B **63**, 214402 (2001).
[32] S. Mori, C.H. Chen, and S.-W. Cheong, Nature (London) **392**, 473 (1998).
[33] P.G. Radaelli, R.M. Ibberson, D.N. Argyriou, H. Casalta, K.H. Andersen, S.-W. Cheong, and J.F. Mitchell, Phys. Rev. B **63**, 172419 (2001).
[34] M. Uehara, S. Mori, C.H. Chen, and S.-W. Cheong, Nature (London) **399**, 560 (1999).
[35] M. Fäth, S. Freisem, A.A. Menovsky, Y. Tomioka, J. Aarts, and J.A. Mydosh, Science **285**, 1540 (1999).
[36] M. Paraskevopoulos, F. Mayr, J. Hemberger, A. Loidl, R. Heichele, D. Maurer, V. Müller, A.A. Mukhin, and A.M. Balbashov, J. Phys.: Condens. Matter **12**, 3993 (2000).
[37] G.-L. Liu, J.-S. Zhou, and J.B. Goodenough, Phys. Rev. B **64**, 144414 (2001).
[38] M. Hennion, F. Moussa, G. Biotteau, J. Rodríguez-Carvajal, L. Pinsard, and A. Revcolevschi, Phys. Rev. B **61**, 9513 (2000).
[39] G. Biotteau, M. Hennion, F. Moussa, J. Rodríguez-Carvajal, L. Pinsard, A. Revcolevschi, Y.M. Mukovskii, and D. Shulyatev, Phys. Rev. B **64**, 104421 (2001).
[40] M. Hennion, F. Moussa, G. Biotteau, J. Rodríguez-Carvajal, L. Pinsard, and A. Revcolevschi, Phys. Rev. Lett. **81**, 1957 (1998).
[41] G. Allodi, R. De Renzi, G. Guidi, F. Licci, and M.W. Pieper, Phys. Rev. B **56**, 6036 (1997).
[42] G. Allodi, R. De Renzi, and G. Guidi, Phys. Rev. B **57**, 1024 (1998).
[43] K. Kumagai, A. Iwai, Y. Tomioka, H. Kuwahara, Y. Tokura, and A. Yakubovskii, Phys. Rev. B **59**, 97 (1999).
[44] M.M. Savosta, P. Novák, M. Maryško, Z. Jirák, J. Hejtmánek, J. Englich, J. Kohout, C. Martin, and B. Raveau, Phys. Rev. B **62**, 9532 (2000).
[45] J.M. Román and J. Soto, Phys. Rev. B **62**, 3300 (2000).
[46] J. Geck, B. Büchner, M. Hücker, R. Klingeler, R. Gross, L. Pinsard-Gaudart, and A. Revcolevschi, Phys. Rev. B **64**, 144430 (2001).
[47] A.M. Balbashov, S.G. Karabashev, Ya.M. Mukovskii, and S.A. Zverkov, J. Cryst. Growth **167**, 365 (1996).
[48] A.A. Mukhin, V.Yu. Ivanov, V.D. Travkin, S.P. Lebedev, A. Pimenov, A. Loidl, and A.M. Balbashov, Pis'ma Zh. Éksp. Teor. Fiz. **68**, 331 (1998) [JETP Lett. **68**, 356 (1998)].
[49] A. Urushibara, Y. Moritomo, T. Arima, A. Asamitsu, G. Kido, and Y. Tokura, Phys. Rev. B **51**, 14 103 (1995).
[50] Y. Moritomo, A. Asamitsu, and Y. Tokura, Phys. Rev. B **56**, 12 190 (1997).
[51] A. Pimenov, Ch. Hartinger, A. Loidl, A.A. Mukhin, V.Yu. Ivanov, and A.M. Balbashov, Phys. Rev. B **59**, 12 419 (1999).
[52] M. Paraskevopoulos, F. Mayr, C. Hartinger, A. Pimenov, J. Hemberger, P. Lunkenheimer, A. Loidl, A.A. Mukhin, V.Yu. Ivanov, and A.M. Balbashov, J. Magn. Magn. Mater. **211**, 118 (2000).
[53] G. V. Kozlov and A. A. Volkov, in *Millimeter and Submillimeter Wave Spectroscopy of Solids*, edited by G. Grüner (Springer, Berlin, 1998), p. 51; A.A. Volkov, Yu.G. Goncharov, G.V. Kozlov, S.P. Lebedev, and A.M. Prochorov, Infrared Phys. **25**, 369 (1985).
[54] F. Dupont, F. Millange, S. de Brion, A. Jánossy, and G. Chouteau, Phys. Rev. B **64**, 220403 (2001).
[55] A. K. Zvezdin and V. A. Kotov, *Modern Magnetooptics and Magnetooptical Materials* (Institute of Physics, Bristol, 1997).
[56] M. Born and E. Wolf, *Principles of Optics* (Pergamon, Oxford, 1986).
[57] A.K. Bogush, V.I. Pavlov, and L.V. Balyko, Cryst. Res. Technol. **18**, 589 (1983).
[58] Y. Yamada, O. Hino, S. Nohdo, R. Kanao, T. Inami, and S. Katano, Phys. Rev. Lett. **77**, 904 (1996).
[59] J.-S. Zhou, J.B. Goodenough, A. Asamitsu, and Y. Tokura, Phys. Rev. Lett. **79**, 3234 (1997).
[60] G. Matsumoto, J. Phys. Soc. Jpn. **29**, 606 (1970).
[61] J. Töpfer and J.B. Goodenough, J. Solid State Chem. **130**, 117 (1997).
[62] S. Foner, in *Magnetism*, edited by G. T. Rado and H. Suhl (Academic Press, New York, 1963), Vol. I, p. 383.
[63] E. A. Turov, *Physical Properties of Magnetically Ordered Crystals* (Academic Press, New York, 1965).
[64] S. Mitsudo, K. Hirano, H. Nojiri, M. Motokawa, K. Hirota, A. Nishizawa, N. Kaneko, and Y. Endoh, J. Magn. Magn. Mater. **177-181**, 877 (1998).
[65] T. Morya, in *Magnetism* (Ref. 62), p. 85.
[66] G.F. Herrmann, J. Phys. Chem. Solids **24**, 597 (1963); Phys. Rev. **133**, A1334 (1964).
[67] G. Cinader, Phys. Rev. **155**, 453 (1967).
[68] A. A. Mukhin, M. Biberacher, and A. Pimenov (unpublished).
[69] V.A. Ivanshin, J. Deisenhofer, H.-A. Krug von Nidda, A. Loidl, A.A. Mukhin, A.M. Balbashov, and M.V. Eremin, Phys. Rev. B **61**, 6213 (2000).
[70] J. Deisenhofer, M.V. Eremin, D.V. Zakharov, V.A. Ivanshin, R.M. Eremina, H.-A. Krug von Nidda, A.A. Mukhin, A.M. Balbashov, and A. Loidl, Phys. Rev. B **65**, 104440 (2002).
[71] A.A. Mukhin, V.D. Travkin, S.P. Lebedev, A.S. Prokhorov, A.M. Balbashov, and I.Yu. Parsegov, J. Phys. IV **7**, 713 (1997); A.A. Mukhin, V.D. Travkin, S.P. Lebedev, A.S. Prokhorov, and A.M. Balbashov, J. Magn. Magn. Mater. **183**, 157 (1998).
[72] R.L. Walker, Phys. Rev. **105**, 390 (1957); P. Fletcher, I.H. Solt, Jr., and R. Bell, *ibid.* **114**, 739 (1959); R.W. Damon and J.R. Eshbach, J. Phys. Chem. Solids **19**, 308 (1961); for a review, see P. Röschmann and H. Dötsch, Phys. Status Solidi B **82**, 11 (1977).
[73] A. H. Morrish, *The Physical Principles of Magnetism* (Wiley, New York, 1965), p. 556.
[74] S.T. Wang and C.W. Searle, Can. J. Phys. **49**, 387 (1971); S.E. Lofland, V. Ray, P.H. Kim, S.M. Bhagat, M.A. Manheimer, and

S.D. Tyagi, Phys. Rev. B **55**, 2749 (1997); A. Schwartz, M. Scheffler, and S.M. Anlage, *ibid.* **61**, R870 (2000).

[75] S.E. Lofland, V. Ray, P.H. Kim, S.M. Bhagat, K. Ghosh, R.L. Greene, S.G. Karabashev, D.A. Shulyatev, A.A. Arsenov, and Y. Mukovskii, J. Phys.: Condens. Matter **9**, L633 (1997).

[76] N.A. Viglin, S.V. Naumov, and Ya.M. Mukovskiĭ, Fiz. Tverd. Tela **43**, 1855 (2001) [Phys. Solid State **43**, 1934 (2001)].

[77] J.-S. Zhou and J.B. Goodenough, Phys. Rev. B **64**, 024421 (2001).

[78] L. Vasiliu-Doloc, J.W. Lynn, A.H. Moudden, A.M. de Leon-Guevara, and A. Revcolevschi, Phys. Rev. B **58**, 14 913 (1998).

[79] E. L. Nagaev, *Physics of Magnetic Semiconductors* (Mir, Moscow, 1979); M.Yu. Kagan, D.I. Khomskii, and M.V. Mostovoy, Eur. Phys. J. B **12**, 217 (1999).